

**EARTHQUAKE RECORD INTERPRETATION FOR SOIL-STRUCTURE INTERACTIONS EFFECTS OF TWO INSTRUMENTED BUILDINGS**

Christine A. Goulet<sup>1</sup>, Atsushi Mikami<sup>2</sup> and Jonathan Stewart<sup>3</sup>

<sup>1</sup> Pacific Earthquake Engineering Research Center, University of California, Berkeley

<sup>2</sup> Department of Civil and Environmental Engineering, University of Tokushima, Tokushima, Japan

<sup>3</sup> Civil & Environmental Engineering Dept., University of California, Los Angeles

**Abstract**

Kinematic soil-structure interaction (SSI) results from the incoherent nature of ground motions, which causes the motions of foundation slabs to generally be reduced from those in the free-field at high frequencies. We compare two models of kinematic SSI utilized in engineering practice: one based on finite element analysis and the second based on a semi-empirical approach. Predictions from both approaches are compared for two well-instrumented structures to observed transfer functions. The results show (1) the two models produce very similar transfer function estimates and (2) the model predictions are generally consistent with observations.

**Introduction**

It has long been recognized that foundation-level and free-field seismic ground motions have different characteristics as a result of the spatial variations in ground motions, even on sites with relatively uniform site conditions (e.g., Yamahara, 1970; Scanlan, 1976; Newmark et al., 1977). The spatial variation of ground motions in the horizontal plane causes foundation motions to be reduced in amplitude relative to free-field motions, an effect termed “base slab averaging”. Likewise, the spatial variation of ground motions vertically leads to an “embedment effect”. Both base slab averaging and embedment are kinematic soil-structure interaction (SSI) effects that influence foundation-level ground motions.

Two types of models have been independently developed over the years to predict kinematic SSI effects. The first is implemented in the computer program SASSI (a System for Analysis of Soil-Structure Interaction; Lysmer et al., 1981, 1999; Ostadan, 2005). SASSI computes the relative motion of the foundation to the free-field (input motion) in terms of a transfer function expressing the frequency-dependent ratio of foundation motion amplitude to free-field motion amplitude. Recent versions of SASSI (Ostadan, 2005; Ostadan and Dang, 2007) allow the free-field motion to have a specified level of coherency (producing spatial variation in phase angles). The second approach for prediction of transfer functions from base slab averaging is based on a theoretical solution by Veletsos and co-workers (1989, 1997) coupled with empirical calibration of an incoherence parameter by Kim and Stewart (2003). The Kim and Stewart approach includes both base slab averaging and embedment effects.

In this paper we compare predictions from the SASSI and semi-empirical models for the conditions present at two instrumented buildings: the Factor building in Los Angeles, California and the Atwood building in Anchorage, Alaska. Both buildings are well suited to these analyses for several reasons:

- i. The buildings have shallow foundations (mat, footing and grade beam) appropriate for use with the kinematic SSI models;
- ii. The buildings consist of moment-resisting steel frames that are not conducive to significant inertial SSI effects, thus simplifying data interpretation for kinematic effects;
- iii. The buildings are well instrumented, including foundation sensors and nearby reference arrays with both surface and downhole high resolution sensors; and
- iv. Data have been recorded during multiple events, allowing investigation of event-to-event variability.

A limitation of the data is that strong shaking has not been recorded. Hence, the structures' responses are essentially in their elastic range; the noise levels are also high, occasionally leading to low signal-to-noise ratios.

Our motivation for these comparisons is to (1) investigate the degree to which the results from the two kinematic SSI models differ from each other and from data and (2) to add new data points to the empirical data set available for the calibration of the semi-empirical model.

### Site and Building Descriptions

#### Factor Building

The Doris and Louis Factor Health Science building is a 17-story special moment-resisting steel frame structure located on the University of California, Los Angeles campus (UCLA). As shown in Figure 1, the building has 15 stories above ground and two basement levels. The Factor building was constructed in the 1970s and was designed under the 1973 building code. It has a footprint of approximately 22.4 m by 38.6 m (73.5 ft by 126.5 ft) from the top basement floor to the 9th floor inclusively. The lower basement (level B) has a smaller footprint of 22.4 m by 29.7 m (73.5 by 97.5 ft). A diagonally-braced overhang at floors 10-15 increases the East-West dimension by 7.4 m (24.2 ft) on the west side and by 3.2 m (10.5 ft) on the east side. The ground surface has a gradient uphill towards the north side, making the first floor at the ground surface on the south side and the second floor at the ground surface on the north side. The building rests on shallow foundations. Figure 1 shows the underlying soil conditions, which consist of Pleistocene alluvium ranging from sands to clays having  $V_s \approx 400$ -600 m/s beneath the foundation.

The Factor building was instrumented following the 1994 Northridge earthquake with a 72-channel sensor array configured as shown in Figure 1. The array includes vertical sensors on the foundation that enable evaluation of rocking in the east-west direction. A 100 m deep vertical array configured with triaxial accelerometers at 100m depth and at the ground surface is located 25 m from the edge of the building in a botanical garden. Additional details on the building and borehole arrays are provided in Goulet et al. (2011).

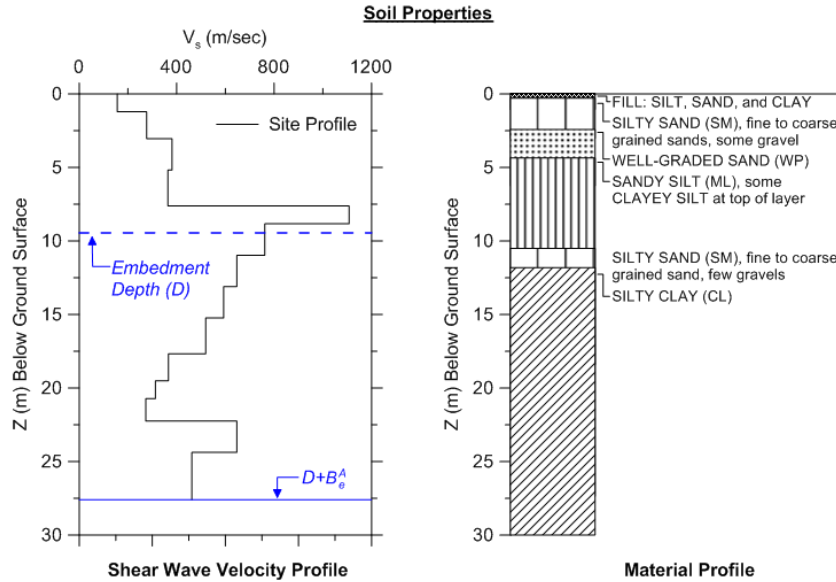
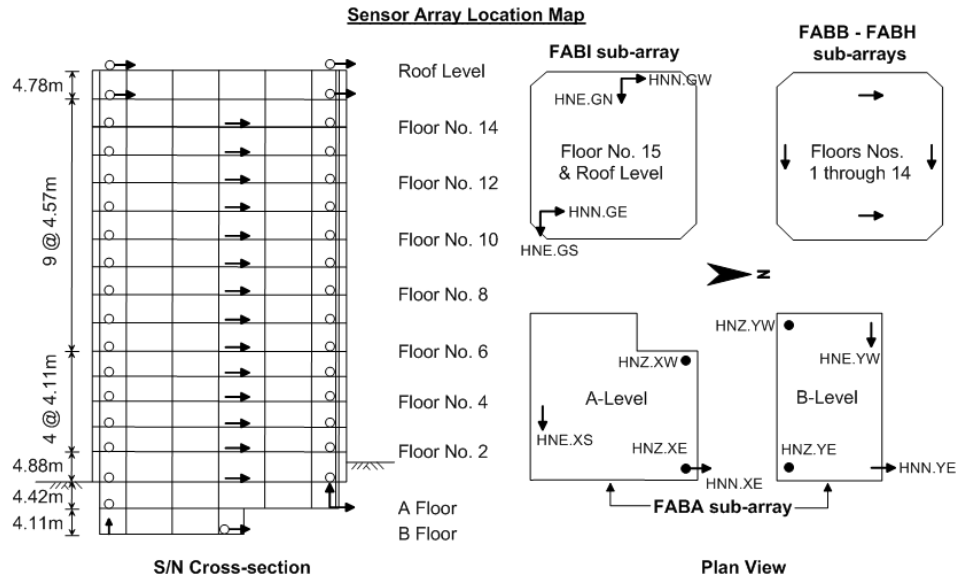


Figure 1. Schematic of the Factor building, showing the sensor array and the subsurface soil profile. Arrows indicate sensor orientation with empty circles pointing into the page and filled circles pointing out of the page. The depths shown on the velocity profile are presented in Table 1. Soil profile information after LeRoy Crandall and Associates, 1976.

### Atwood Building

The Atwood building is a 21-story moment-resisting steel frame structure located in downtown Anchorage, Alaska. As shown in Figure 2, the building has 20 stories above ground and a single basement level. The Atwood building was built in 1980 under the 1979 Uniform Building Code. The Atwood building has a square footprint of 39.6 m (130 ft) with a square concrete core of 14.6 m (48 ft). As shown in Figure 2, the reinforced concrete shallow foundation system consists of a mat under the center core with a perimeter wall footing

connected with grade beams. The foundation is connected to that of the adjacent plaza by grade beams.

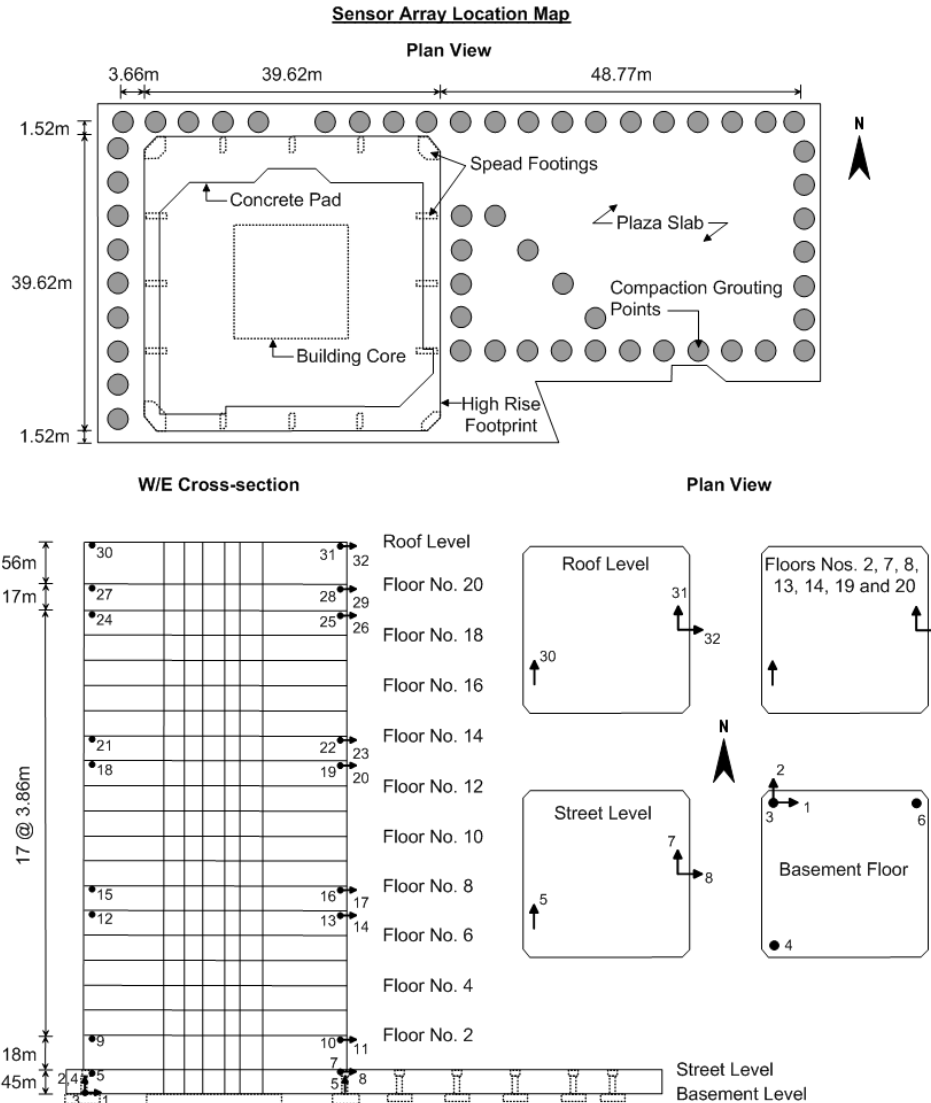


Figure 2. Schematic of the Atwood building, showing the sensor array. Arrows indicate sensor orientation with empty circles pointing into the page and filled circles pointing out of the page.

Figure 3 shows the underlying soil conditions, which consist of a thick soil layer of the Bootlegger Cove Formation with an average thickness of about 30 m in the vicinity of the site. This geologic formation is mostly composed of silty materials deposited in a late Pleistocene glaciomarine-glaciodeltaic environment (Ulery et al., 1983). We were unable to locate site-specific boreholes or geophysical logs for the Atwood building, and the site conditions are taken from a borehole at the Delaney Park site (the location of the free-field array) 165 m from the Atwood building. Even at the borehole location, there are no geophysical measurements, but  $V_s$  profiles have been estimated by Nath et al. (1997) and Yang et al. (2008) from inversion of array data, with the results shown in Figure 3.

The instrumentation system, consisting of structural and borehole arrays, was installed in 2003. As shown in Figure 2, the structural instrumentation is composed of 32 accelerometers distributed on 10 of the 21 floors of the structure. The two basement floors have three vertical sensors each that allow computation of rotation in both directions. A 30.5 m deep vertical array of six sensors distributed at depth plus one at the surface is located approximately 165 m from the Atwood building at Delaney Park. The surface sensor is used as the free-field motion. Further details on the instrumentation system are provided in Çelebi (2003; 2006).

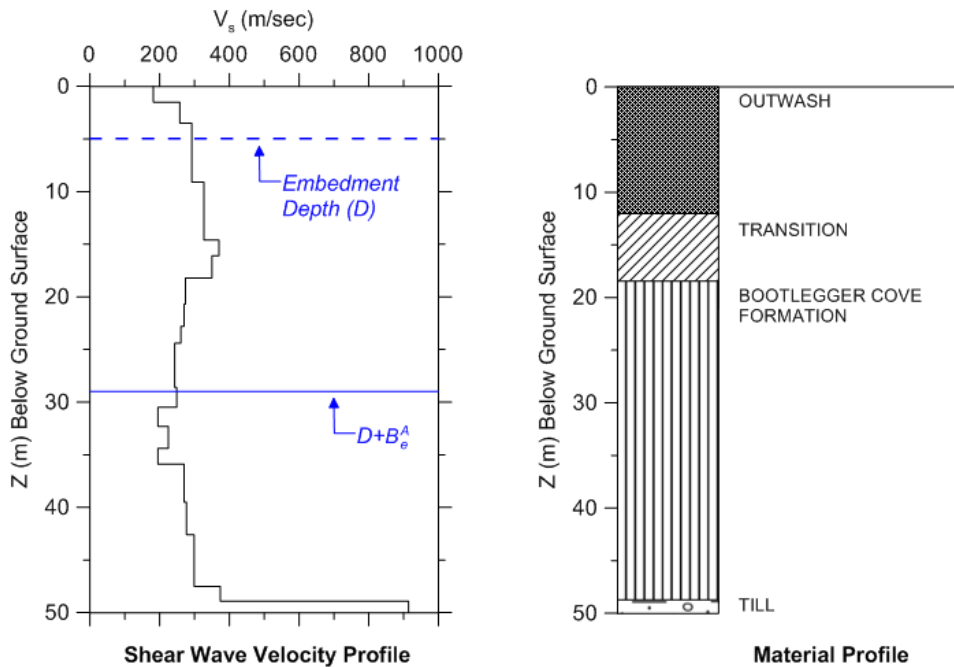


Figure 3. Shear wave velocity profile at the location of the borehole array in Delaney Park after Nath et al. 1997 and Yang et al., 2008. The depths shown on the velocity profile presented in Table 1. The borehole array is about 165 m (540 ft) away from the Atwood building.

### Modal Properties

We performed system identification analyses similar to those described in Stewart and Fenves (1998) to identify fixed- and flexible-base modal parameters for the Factor and Atwood buildings. Modal parameters for the two base fixity conditions were nearly identical, indicating period lengthening near unity and practically zero foundation damping. This is expected, as the ratio of structure to soil stiffness  $h/(V_s T)$  (where  $h$  = height to centroid of first mode shape,  $V_s$  = soil shear wave velocity, and  $T$  = structure fixed base period) is very small (0.10 for Factor, 0.07 for Atwood), so inertial SSI effects are expected to be minimal per classical method such as those in Veletsos and Nair (1975). The details of these analyses are presented in Goulet et al. (2011). In the remainder of this article, we focus on kinematic interaction effects for the two buildings, which are expected to be more significant as a result of their embedment and large foundation area.

**Model-Based Kinematic Transfer Functions**

**Semi-Empirical Model**

Veletsos and co-workers (1989, 1997) developed models for theoretical base slab averaging that combine an analytical representation of the spatial variation of ground motion with rigorous treatment of foundation-soil contact. Kim and Stewart (2003) calibrated Veletsos’ analysis procedure against observed foundation/free-field ground motion variations as quantified by frequency-dependent transfer functions. Two types of transfer functions can be computed from the models presented by Veletsos and co-workers:

$$H_u(\omega) = \frac{u_{FIM}}{u_g} \quad H_\theta(\omega) = \frac{\theta_{FIM}L}{u_g} \quad (1)$$

where  $u_{FIM}$  denotes foundation translation,  $u_g$  is the ground motion translation in the same direction,  $\theta_{FIM}$  denotes kinematic rotation about an axis normal to the direction of  $u_{FIM}$  and  $u_g$ , and  $L$  is the foundation half dimension in the same direction as  $u_{FIM}$  and  $u_g$ . The acronym ‘FIM’ indicates Foundation Input Motion, which is the motion of the foundation for the hypothetical condition of no inertia (in the structure or foundation). Motions recorded on actual foundations, which naturally have inertia, represent an approximation of FIM. Similarly, the acronym FFM is used to represent the free-field motion.

The Kim and Stewart calibration considered the horizontal translation transfer function only ( $H_u$ ), and resulted in apparent  $\kappa$  values (denoted  $\kappa_a$ ) for each structure/data set combination. Those  $\kappa_a$  values reflect not only incoherence effects, but necessarily also include average foundation flexibility and wave inclination effects for the calibration data set. Kim and Stewart’s analyses were for 29 sites having structure/free-field arrays similar to those for Atwood and Factor, although with lower quality sensors and data acquisition systems (e.g., much of the data were from analogue systems). The Kim and Stewart model is of particular interest because its recommendations form the basis of seismic guidelines for retrofit of existing buildings (e.g., ASCE 2007; updated in NIST CJV, 2012).

Table 1 lists the model input parameters required to apply the semi-empirical base slab averaging model and embedment model from Kim and Stewart (2003). Those parameters are based on the foundation dimensions and on the shear wave velocity profile over the embedment depth of the foundation and to a depth of  $B_e^A = \sqrt{A_f}/4$  below the foundation.

Table 1. Input parameters to the Kim and Stewart (2003) semi-empirical model

| <i>Parameter</i>   | <i>Factor</i> | <i>Atwood</i> |
|--|---------------|---------------|
| Embedment Depth ( $D$ )* (m)                                     | 9.5           | 5.0           |
| Area of Foundation ( $A_f$ ) ( $m^2$ )                           | 1034          | 1822          |
| Effective Foundation Size ( $B_e^A$ ) (m)                        | 18.1          | 24.1          |
| Average $V_s$ to Embedment Depth, $D$ * (m/s)                    | 427           | 243           |
| Average $V_s$ from Base of Foundation $D$ to $D + B_e^A$ * (m/s) | 492           | 291           |

\* The depths and the shear wave velocity profiles are shown in Figures 1 and 3 for the Factor and Atwood buildings, respectively.

### Finite Element Model in SASSI

SASSI was originally developed by Lysmer et al. (1981, 1999) and utilized the substructure approach in which the linear SSI problem is divided into sub problems based on the principle of superposition using linear material properties. Soil is assumed to consist of horizontal layers overlying either a rigid base or an elastic half-space. The structure and foundation are modeled by finite elements. Foundations are modeled as massless slabs to exclude inertial effects, with a Young's modulus appropriate for concrete. Ostadan and Dang (2007) extended SASSI to include incoherent ground motions that include stochastic phase variations as prescribed by the spatial coherency model of Abrahamson and co-workers (1991, 2005). We utilize this extended version of SASSI in the present analyses.

Figure 3(a) shows the foundation finite element model developed for the Factor building foundation system. Basements A and B were modeled as described in the previous section. Figure 3(b) shows the SASSI finite element model for the Atwood building foundation system.

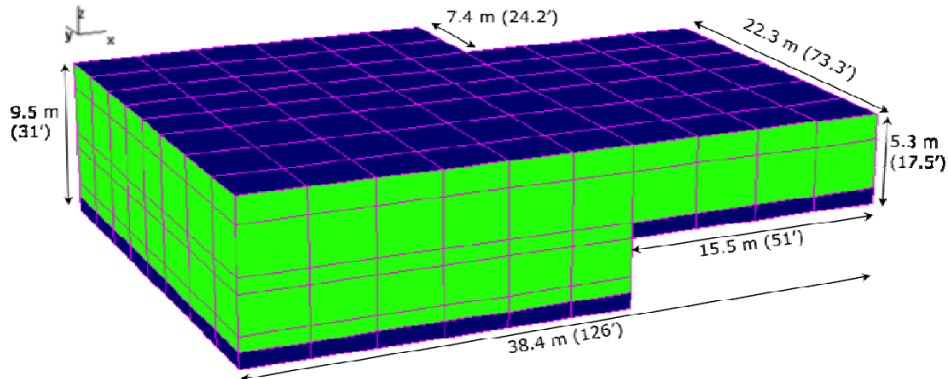


Figure 3(a). SASSI finite element model, Factor building. The positive x axis points to the North.

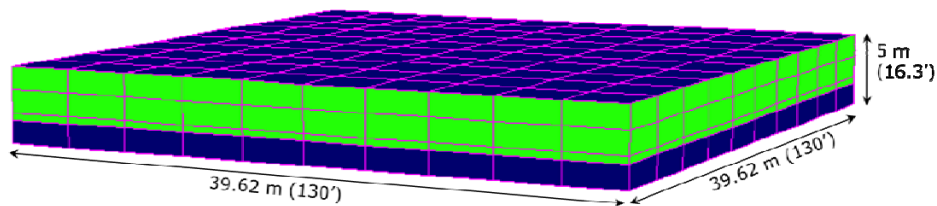


Figure 3(b). SASSI finite element model, Atwood building.

### Model Comparisons for Subject Buildings

Figures 4(a) and (b) compare the transfer functions for the Factor and Atwood buildings as predicted using the semi-empirical and SASSI approaches. In the case of the semi-empirical approach, we show transfer functions for the base slab averaging and embedment effect alone and with the two combined. The combination is through simple multiplication at each respective frequency. Embedment effects are more important than base slab averaging effects for the subject buildings in the frequency ranges of interest (less than approximately 8 Hz). SASSI

results are nearly identical in the two horizontal directions, so only a single direction is shown in the figures.

The combined semi-empirical model (including base slab averaging and embedment effects) provides similar transfer functions to those from SASSI.

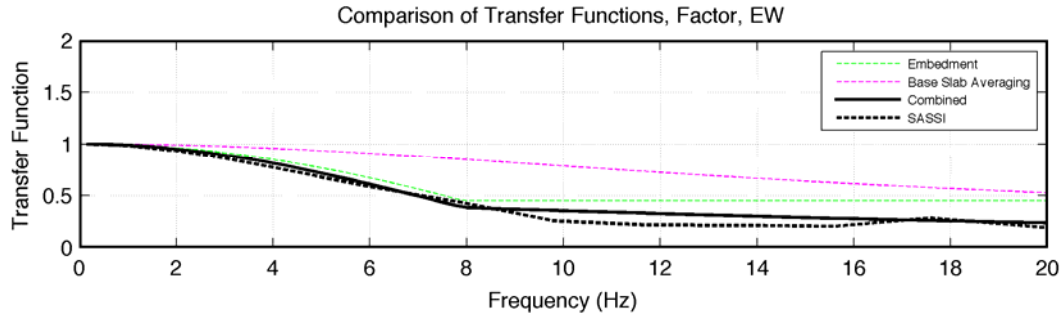


Figure 4(a). Comparison of kinematic transfer functions, Factor building. The EW-NS directions lead to slightly different shapes for the SASSI model (not shown), due to the asymmetry of the foundation plan.

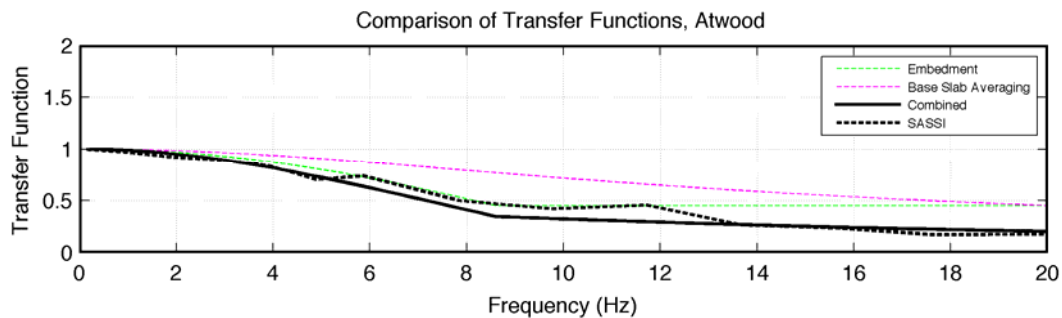


Figure 4(b) Simplified semi-empirical SSI model for kinematic transfer function, Atwood building. Due to the symmetric foundation, the SASSI transfer functions are exactly the same in both directions.

## Kinematic Transfer Functions from Recordings

### *Selection of Recordings*

A large number of events were recorded by both building arrays, but most of the accelerations were of very low amplitude. The event selection criteria used are:

1. Availability of array recordings for basement, roof and free-field.
2. Signal-to-noise ratio as large as possible (a trial of motions indicate satisfactory results generally for peak ground acceleration (PGA) stronger than about 2% g for the free-field records).

For the Factor building, many changes in instrumentation occurred in the 2003-2005 period making it difficult to correctly process the data. Therefore, events recorded after January 2006 were selected, which is a time period for which the instrumentation configuration and sensors naming scheme are best known.

Table 2 lists the selected earthquakes, and the PGA values for the free-field records. As described in Goulet et al. (2011), many more records were analyzed over the course of the project, mostly for system identification analysis of modal vibration properties and to define the usable signal to noise ratio; these results are not reported here for brevity.

Table 2. Selected records for both buildings

| <i>Building</i> | <i>Earthquake ID</i> | <i>Date, Epicentral Location</i>   | $M_w$ | <i>Hypocentral Distance (km)</i> | <i>PGA, Free-Field EW (cm/s<sup>2</sup>)</i> | <i>PGA, Free-Field NS (cm/s<sup>2</sup>)</i> |
|-----------------|----------------------|------------------------------------|-------|----------------------------------|--|--|
| Factor          | 2007/221             | Aug. 9, 2007, Chatsworth           | 4.6   | 31                               | 8.1  | 7.3  |
|                 | 2008/211             | Jul. 29, 2008, Chino Hills         | 5.4   | 64                               | 24.0   | 22.6   |
| Atwood          | 20041108             | Nov. 8, 2004, Denali National Park | 4.9   | 222                              | 2.1  | 1.7  |
|                 | 20050216             | Feb. 16, 2008, Point McKenzie      | 4.7   | 14                               | 11.8   | 10.1   |

### ***Computation Procedures***

The transfer functions in Eq. (1) are frequency-dependent and complex-valued. Typically the phase of the transfer function is not used and the analysis emphasizes transfer function amplitude. This convention is followed and subsequent references to “transfer function” imply the amplitude of the complex-valued ratios.

Recall that the FIM is the theoretical motion of the base slab if the foundation and structure had no mass. The recorded foundation motion has been shown to provide a good estimate of the FIM for frequencies distinct from the fundamental-mode frequencies of vibration of the structure (Kim and Stewart, 2003).

Transfer functions are evaluated from the recordings using procedures described in Mikami et al. (2008). Frequency domain smoothing is applied to spectral density functions for the ‘input’ (denominator in Eq. 1, denoted  $y$ ) and ‘output’ (numerator in Eq. 1, denoted  $x$ ), from which transfer functions are computed as follows:

$$|H(\omega)| = \sqrt{\frac{S_{yy}}{S_{xy}}} \quad (4)$$

where  $S_{yy}$  is the smoothed auto-spectral density functions for the output and  $S_{xy}$  is the cross-spectral density function of the input/output pair. This transfer function formulation represents an average that tends to minimize the impact of noise in the data (Goulet et al. 2011; Ljung, 1999 and Pandit, 1991). The method and degree of smoothing is described further below. In addition, the coherence (square of coherency) of the data is calculated as:

$$\gamma^2(\omega) = \frac{|S_{xy}(\omega)|^2}{S_{xx}(\omega)S_{yy}(\omega)} \quad (5)$$

The coherence varies between zero and one and is used to judge the effects of noise in the data. Frequency ranges in the transfer function that are dominated by noise (typically high frequencies) will have low coherence. Incoherence can be due to noise or to natural physical processes such as wave scattering in the soil.

As described by Mikami et al. (2008), the calculation of transfer and coherence functions for a given record pair is affected by the time windows analyzed (e.g., full record, shear-wave window, etc.) and the method and level of smoothing. Because the window selection is largely subjective, we attempted to make the selection more systematic and reproducible. The approach followed in the present work is as follows:

- The window of time considered in the analysis (time window) was selected using four alternate approaches: subjective selection of strong shaking (encompassing approximately the shear wave window, and sometimes, initial portion of surface waves), and three windows based on the 5-75%, 5-85% and 5-95% significant duration window from normalized Arias Intensity (Arias, 1970). An example of showing a window selection for a record is shown in Figure 5.
- We perform frequency domain smoothing using Hamming windows of width  $2m+1$  applied directly to the power spectral values (larger  $m$  corresponds to more smoothing; we use  $m = 3, 5, 7,$  and  $9$ ). The appearance of the transfer function depends on the level of smoothing and the number of frequencies in the spectral density function (larger for longer duration time series). For a shorter array and a given level of smoothing, the transfer function will effectively be smoother, which affects the interpretation. Although we completed both time-domain and frequency domain smoothing, we focus here on frequency domain smoothing results. Because of the relatively short record durations, sub-dividing short duration records, as in time-domain smoothing, can produce results very sensitive to the level of smoothing.

Transfer functions were computed for the four window widths and four levels of smoothing defined above. Figure 6 shows an example of the transfer and coherence functions produced with this approach. We also show on the coherence plot the predicted median coherence for the FFM-FIM separation distance based on Abrahamson and co-workers (1991, 2005) empirical model (derived from dense arrays of ground stations). Points that correspond to coherence larger or equal to 0.8 are also marked with blue circles on the transfer functions. The shaded region in Figure 6 represents a general interpreted transfer function over the usable bandwidth, which is established by a polynomial regression on the transfer function points. Two regressions were performed: one using only the highly coherent data points (coherence  $> 0.8$ ) and one using all the data points for the selected bandwidth.

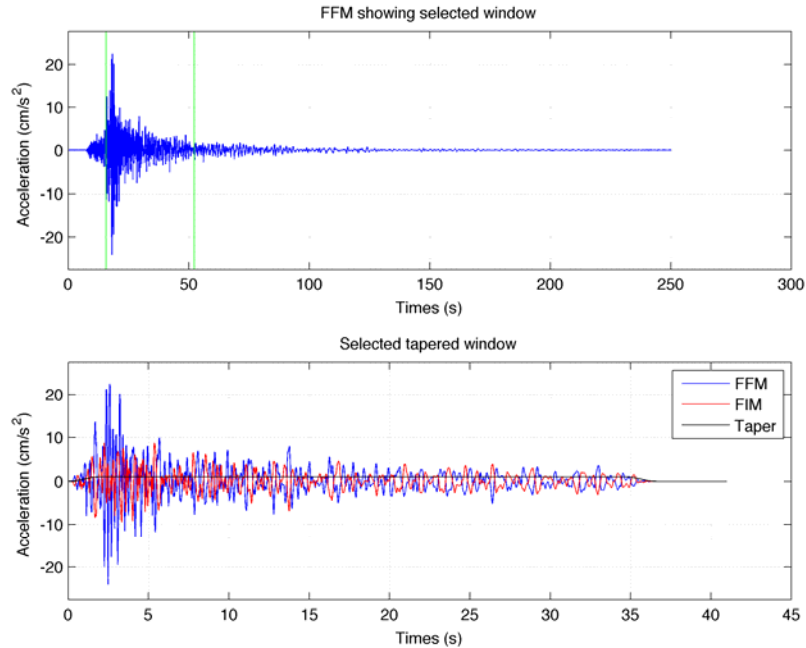


Figure 5. Example of time series window selection based on the FFM input, 2008/211 EW, Factor building. The bottom plot also shows the taper to zero at the beginning and end of the window.

The general transfer function shapes are similar for different window durations and smoothing levels, but the interpretation could be affected as a result of shifting locations of peaks and troughs. The approach adopted here is intended to provide more robust interpretations than would be obtained with strict adoption of a single window duration and smoothing level or from subjective criteria that could vary substantially from record-to-record.

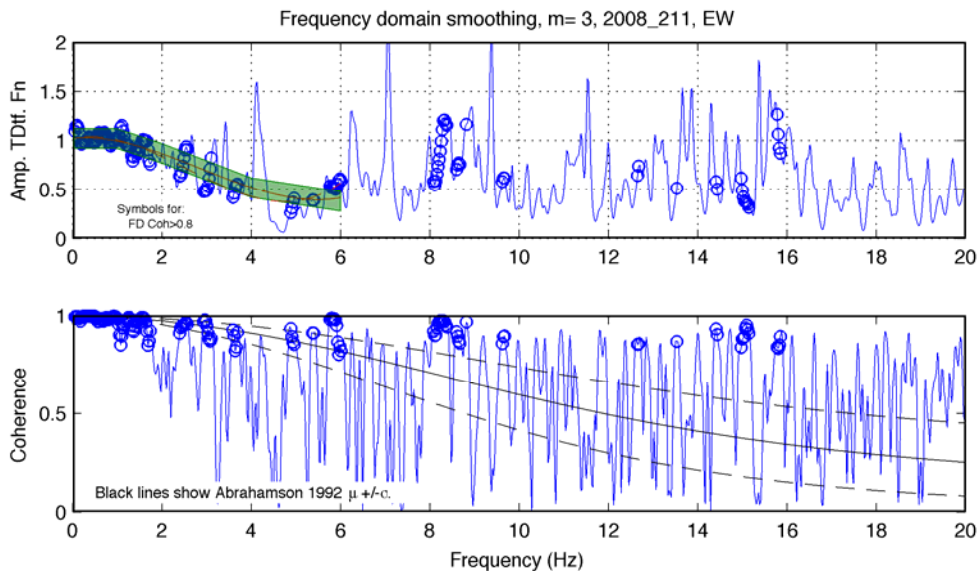


Figure 6. Transfer function and coherence for the 2008/211 EW data set, Factor building. Frequency domain smoothing with 7 points Hamming window.

As pointed out by Mikami et al. (2008), perhaps the most critical element of this procedure is identification of the usable frequency range of the transfer function. The reliability of the transfer function ordinates degrades as coherence falls. At the extreme where the coherence corresponds to that of white noise (frequencies  $> \sim 11$  Hz in Figure 6), the transfer function essentially represents the ratio of two noise signals, and only sampling across very large numbers of records would produce meaningful results. At low frequencies coherence tends to be near unity, and transfer function ordinates are robust, so the practical issue is the maximum usable frequency of the transfer function. We identify the usable frequency range as the range having dense spacing of high coherence ordinates (typically greater than approximately 0.8). At high frequencies, occasional high coherence points can be found, but when widely spaced on the frequency axis, we argue that the transfer function is beyond its useful frequency range. Hence, the maximum usable frequency is that which separates the portion of the frequency spectrum having relatively closely spaced from relatively sparse high frequency ordinates. This judgment is admittedly subjective.

### ***Results for the Factor and Atwood Buildings***

Figures 6 and 7 show selected transfer and coherence functions for the Factor building computed for the two events listed in Table 2 in the EW and NS directions respectively. The jagged blue lines show the transfer function and coherence computed for a specified window and level of smoothing, as given in the caption, whereas the shaded green area is the best-fit interpretation over the usable frequency range derived from multiple computations with variable levels of smoothing as described above. The regression curves used to constrain the green shaded area are shown in Figure 6 by the red solid and dashed lines for all and only the high coherence data respectively. Blue circles are used to highlight ordinates for which the coherence is larger than 0.8. The Abrahamson and co-workers (1991, 2005) coherence model is shown for reference in the coherence plots.

The maximum usable frequency is taken as 6 Hz in the EW direction and 8 Hz in the NS direction based on the spacing of high coherence data points (narrow at lower frequencies, wide at higher frequencies). Note that the loss of coherence at 6-8 Hz is unrelated to the data acquisition system in this case, which has a wide bandwidth. The loss of coherence is a natural process that is fully expected for accelerometers at distinct locations, as reflected by the median coherence prediction (from Abrahamson and co-workers, 1991 and 2005) shown in the plots, which follows the same general trend as the data. Similar values of limiting frequencies have been encountered in previous work for other structures (Kim and Stewart 2003; Mikami et al. 2008).

A consistent peak and trough pair in the 4-5 Hz frequency range is visible for the 2008/211 EW earthquake dataset (Figure 6). This is not observed in the NS transfer functions for the same earthquake or in the 2007/221 dataset (Figure 7). It is unclear what causes this feature.

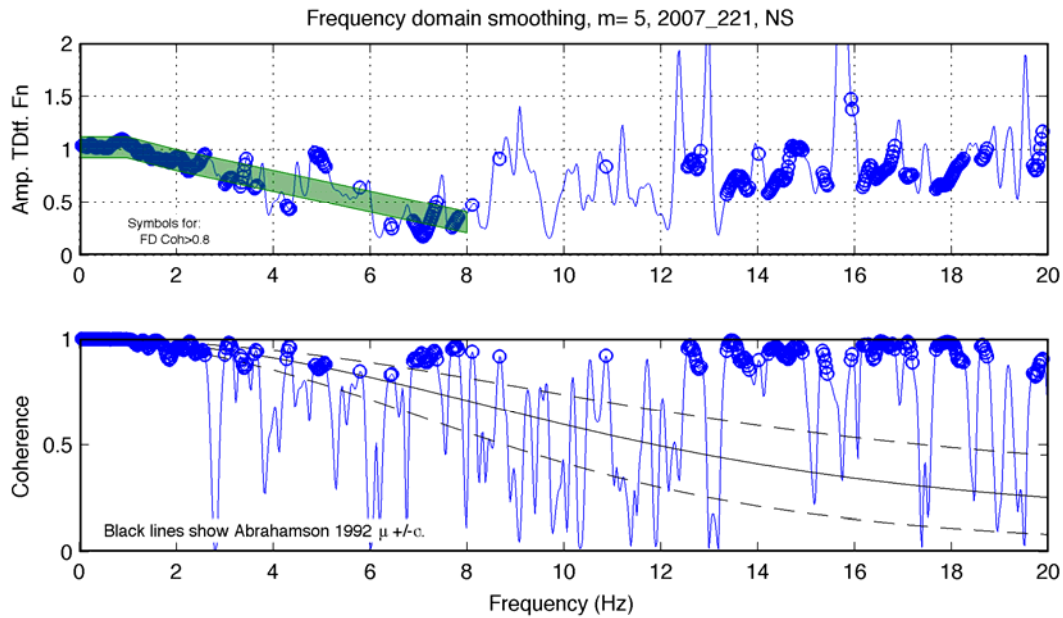


Figure 7. Transfer function and coherence for the 2007/221 NS data set, Factor building.

Sample results for the Atwood building are presented in Figures 8-9 in the same format. Using data from the two earthquakes listed in Table 2. The relatively large separation distance between the FFM and FIM (165 m) results in relatively rapid decay of coherence with frequency. If the transfer function interpretations were performed only with high coherence data, the maximum frequency would be in the range of 1-1.5 Hz. Nonetheless, transfer function ordinates at higher frequencies are stable under different levels of smoothing up to approximately 8 Hz or more and are reasonably consistent between components for the two events considered. Nonetheless, due to the large impact of noise, the transfer function ordinates should be viewed as few samples of an essentially random process, and it is unlikely that they accurately reflect the mean of the underlying physical process (i.e., the kinematic transfer function).

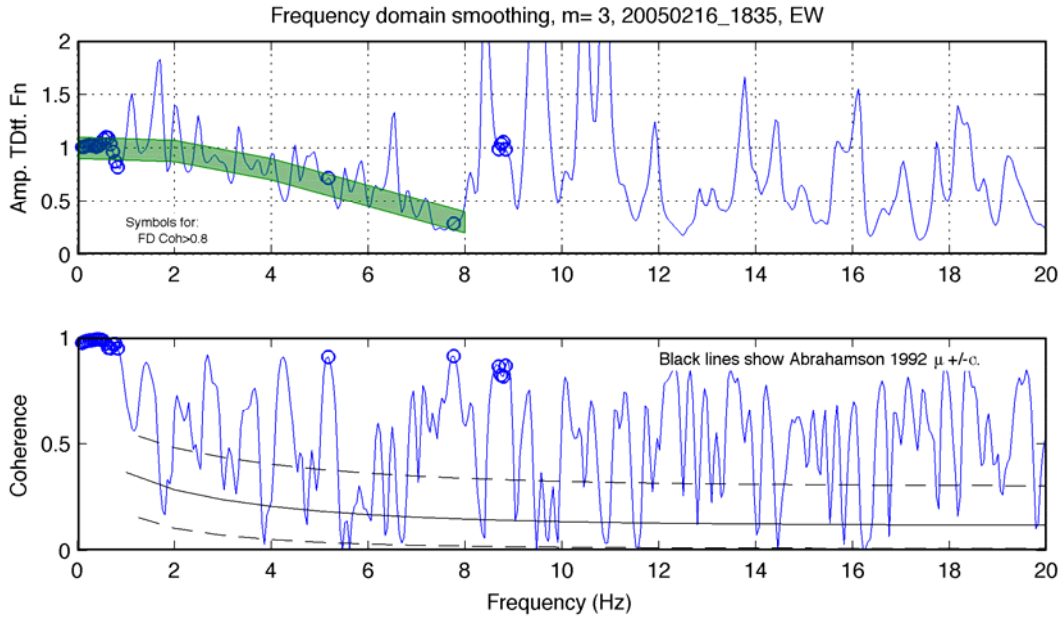


Figure 8. Transfer function and coherence for the 20050216 EW data set, Atwood building.

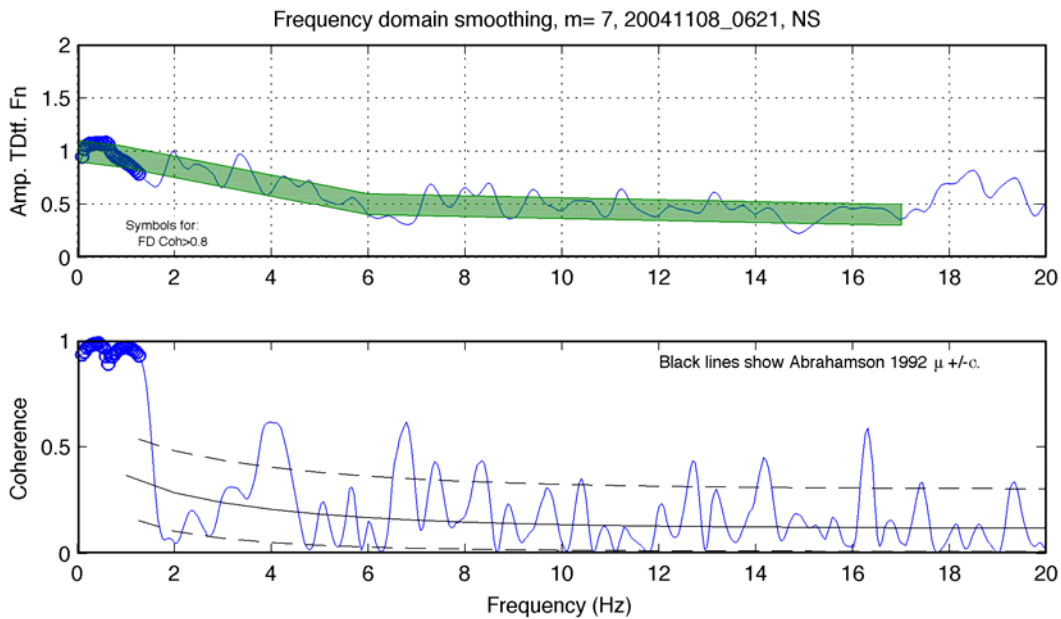


Figure 9. Transfer function and coherence for the 20041108 NS data set, Atwood building.

### Interpretation and Discussion

As shown previously in Figure 4, the SASSI and semi-empirical models for kinematic SSI provide very similar estimates of transfer functions. Figures 10-13 compare those estimates to the transfer functions from data. We show transfer function bands for each earthquake at each site that envelop the component-specific bands presented previously. The data tend to agree, in a general sense, with the model predictions, keeping in mind that the data-based transfer functions are represented by bands rather than single lines.

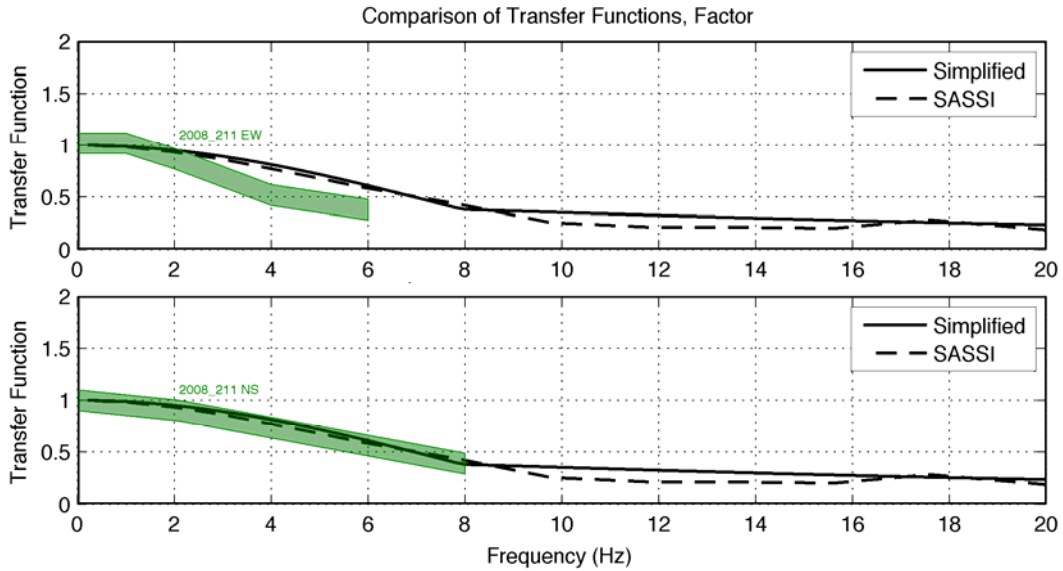


Figure 10. Comparison of transfer functions, 2008/211 earthquake data, Factor building. EW component on top, NS component on bottom.

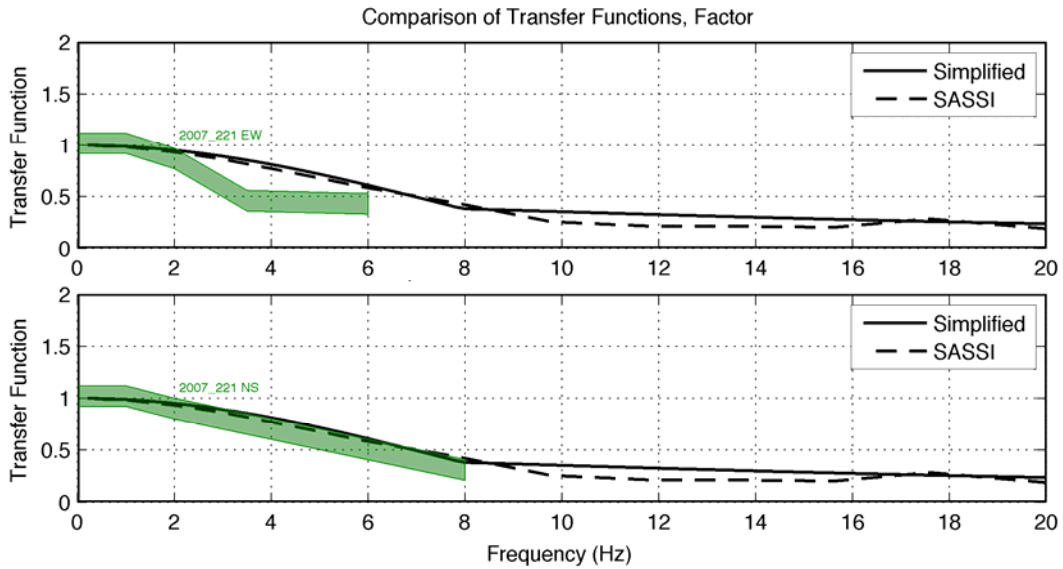


Figure 11. Comparison of transfer functions, 2007/221 earthquake data, Factor building. EW component on top, NS component on bottom.

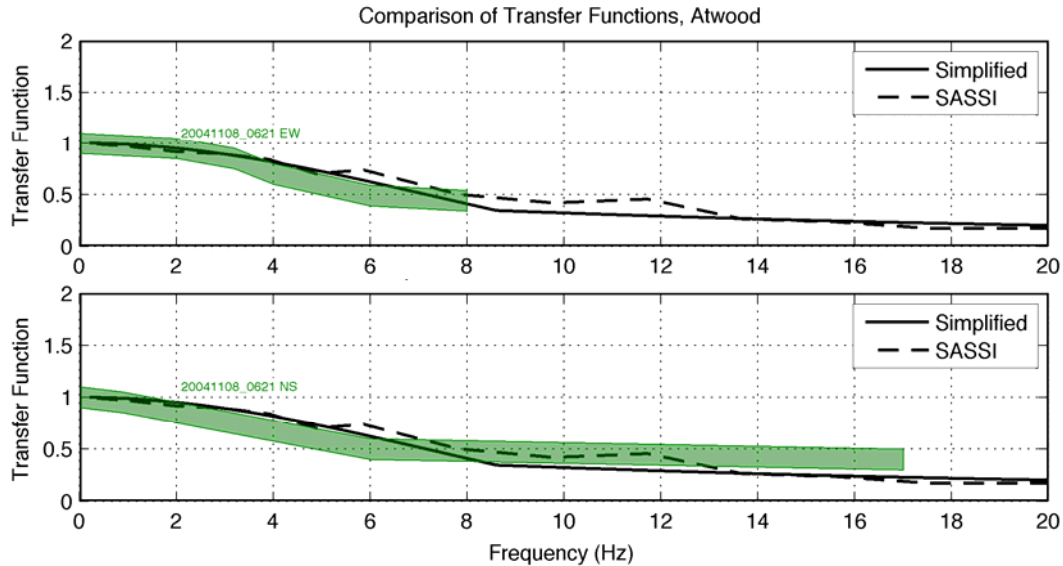


Figure 12. Comparison of transfer functions, 20041108 earthquake data, Atwood building. EW component on top, NS component on bottom.

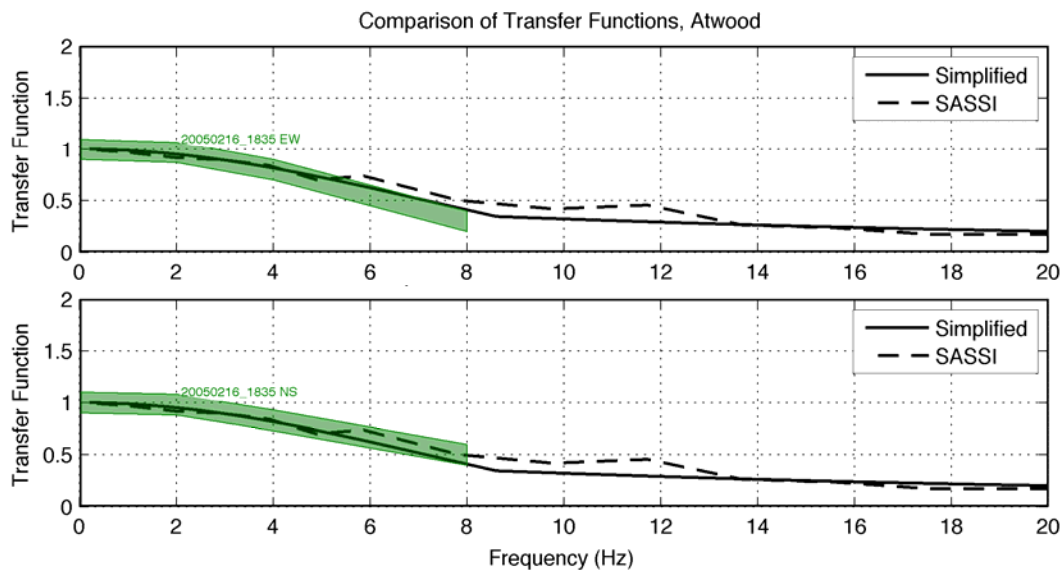


Figure 13. Comparison of transfer functions, 20050216 earthquake data, Atwood building. EW component on top, NS component on bottom.

A significant source of uncertainty affecting the data interpretation that could be reduced with further optimization of the array set are the geophysical data at the sites and the instrument spacings. As described previously, high quality geotechnical and geophysical data should ideally be present for both the building and free-field sites. One important issue encountered was the lack of information on the sub-surface geology, either at the building location or at the free field sensor location. This is important because both models considered here (Kim and Stewart, 2003 and SASSI) use the shear wave velocity as input. In order to allow a fair comparison of data and models, it would be important to have the detailed shear wave velocity profile around and under the buildings and at the free field station. The quantification of differences in shear wave velocity profiles at both locations would bring insight to the results interpretation, by allowing

the understanding of site response effects. For Factor, both shear wave velocity profiles were obtained (building and free-field station location), although accurate elevation datum was not available to relate the two profiles. For the Atwood building location, soil profile information was not available. The only profile available was derived from seismic wave inversion at the free-field array location. If site conditions at the two locations were significantly different, variable levels of site response could be mistakenly interpreted as a kinematic interaction effect. Reduced instrument spacing, especially for the Atwood building, would improve the coherence of the signals and improve the confidence in the transfer function ordinates. Further recommendations on instrument layout to improve the ability to infer SSI effects (both kinematic and inertial) are provided in Goulet et al. (2011). Nonetheless, we find that the data-based results obtained through this work are consistent with the two models considered.

### Acknowledgments

Funding for this work was provided by the Data Interpretation Project of the California Strong Motion Instrumentation Program, California Geological Survey, Agreement No. 1008-920. The authors would like to thank the Strong Motion Instrumentation Program and the Ground Response Subcommittee panel who provided insightful comments throughout the project.

Strong motion recordings for the project were provided by Chris Stephens from the U.S. Geological Survey and by Monica Koehler from Caltech. We would also like to acknowledge Drs. Robert Nigbor, Derek Skolnik, Mehmet Çelebi and Jamie Steidl for their help and guidance regarding the available data for this study.

### References

- Abrahamson, N.A., Schneider, J.F., and Stepp, J.C. (1991). "Empirical spatial coherency functions for application to soil-structure interaction analyses", *Earthquake Spectra*, 7, 1-26.
- Abrahamson, N. A., (2005). "Updated coherency model", Report prepared for Bechtel Corporation.
- American Society of Civil Engineers (2007). "ASCE 41-06: Seismic Rehabilitation of Existing Buildings", American Society of Civil Engineers, 416 p.
- Arias, A. (1970). "A Measure of Earthquake Intensity", R.J. Hansen, ed. *Seismic Design for Nuclear Power Plants*, MIT Press, Cambridge, Massachusetts, pp. 438-483.
- Çelebi, M. (2006). "Recorded earthquake responses from the integrated seismic monitoring network of the Atwood Building, Anchorage, Alaska", *Earthquake Spectra*, v. 22, no. 4, p. 847-864.
- Çelebi, M. (2003). "Seismic Instrumentation Plan for Robert B. Atwood Building, Anchorage, AK 99501", Administrative Report, U.S. Geological Survey.

Goulet, C.A., Stewart, J.S. and Mikami, A. (2011). "Earthquake Record Interpretation and Soil-Foundation Structure Interaction Effects for the Atwood and Factor Buildings", California Strong Motion Instrumentation Program, Sacramento, Final Report, 60 pp.

Kim, S. and Stewart, J.P. (2003). "Kinematic soil-structure interaction from strong motion recordings," *J. Geotech. & Geoenv. Engrg.*, ASCE, 129 (4), 323-335.

LeRoy Crandall and Associates Consulting Geotechnical Engineers (1976). "Report of Foundation Investigation and Site Response Study, Proposed Cancer Center/School of Nursing, Tiverton and South Circle Drives, Los Angeles, California for the University of California, Los Angeles", Campus Capital Programs building archives, University of California, Los Angeles.

Ljung, L. (1999). "System identification: Theory for the user", 2nd Ed., Prentice Hall, Englewood Cliffs, NJ.

Lysmer, J., M. Tabatabaie-Raissi, F. Tajirian, S. Vahdani, and Ostadan F. (1981), "SASSI-A System for Analysis of Soil-Structure Interaction," Report no. UCB/GT/81-02, Department of Civil Engineering, University of California, Berkeley.

Lysmer, J., Ostadan F. and Chin, C. (1999). "SASSI2000 Theoretical Manual."

Mikami, A., Stewart, J.P., and Kamiyama, M. (2008). "Effects of time series analysis protocols on transfer functions calculated from earthquake accelerograms", *Soil Dynamics and Earthquake Engineering*, 28 (9), 695-706.

Nath, S. K., Chatterjee, D., Biswas, N. N., Dravinski, M., Cole, D.A., Papageorgiou, A., Rodriguez, J.A., and Poran, C.J. (1997). "Correlation study of shear wave velocity in near surface geological formations in Anchorage, Alaska", *Earthquake Spectra* 13(1) 55-75.

NEHRP Consultants Joint Venture, 2012. Soil-Structure Interaction for Building Structures, Report NIST/GCR 11-917-14, National Institute of Standards and Technology, Washington, D.C

Newmark, N.M., Hall, W.J., and Morgan, J.R. (1977). "Comparison of building response and free field motion in earthquake," *Proc. 6th World Conf. Earthquake Engrg.*, New Delhi, India, Vol. II, 972-978.

Ostadan, F. (2005). Soil-structure interaction analysis including ground motion incoherency effects, 18th International Conference on Structural Mechanics in Reactor Technology (SMiRT 18), Beijing, China.

Ostadan, F. and Dang, N. (2007), "SASSI-SRSS Approach for SSI Analysis with Incoherent Ground Motions", Bechtel National, San Francisco, California.

Pandit, S.M. (1991). "Modal and Spectrum Analysis", John Wiley, New York, NY.

Scanlan, R.H. (1976). "Seismic wave effects on soil-structure interaction," J. Earthquake Engrg. Struct. Dynamics, 4, 379-388.

Stewart, J. P., and Fenves, G. L. (1998). "System identification for evaluating soil-structure interaction effects in buildings from strong motion recordings", J. Earthquake Engrg. Struct. Dyn., 27, 869–885.

Ulery, C.A., Updike, R.G., and USGS Office of Earthquakes (1983). "Subsurface structure of the cohesive facies of the Bootlegger Cove formation, southwest Anchorage: Alaska", Division of Geological & Geophysical Surveys Professional Report 84, 5 p., 3 sheets, scale 1:15,840.

Veletsos, A. S., and Nair, V. V. (1975). "Seismic interaction of structures on hysteretic foundations", J. Struct. Eng., 101, 109–129.

Veletsos, A.S. and Prasad, A.M. (1989). Seismic Interaction of Structures and Soils: Stochastic Approach, ASCE Journal of Structural Engineering, Vol. 115, pp. 935-956.

Yamahara, H. (1970). "Ground motions during earthquakes and the input loss of earthquake power to an excitation of buildings," Soils and Foundations, 10(2), 145-161.

Yang, Z., Dutta, U., Xiong, F., Biswas, N and Benz, H. (2008). "Seasonal frost effects on the dynamic behavior of a twenty-story office building", Cold Regions Sc. & Techn. 51, 76-84.

